Capacitive Imaging for Skin Characterizations and Solvent Penetration Measurements

Xu Zhang, Christos Bontozoglou, Elena Chirikhina, Majella E. Lane and Perry Xiao *

School of Engineering, London South Bank University, 103 Borough Road, London SE1 0AA, UK.

* Corresponding Author, Tel: 00 44 20 7815 7569 Fax: 00 44 20 7815 7561 email: xiaop@lsbu.ac.uk

Abstract

Capacitive contact imaging has shown potential in measuring skin properties including hydration, micro relief analysis, as well as solvent penetration measurements. Through calibration we can also measure the absolute permittivity of the skin, and from absolute permittivity we then work out the absolute solvent content in skin. In this paper, we present our latest study of capacitive contact imaging for skin characterizations and vivo skin solvent penetration. We will show

how to use capacitive occlusion measurements to characterize skin damages, and how to calculate the absolute water content and solvent content in skin.

Keywords

Capacitive imaging, skin hydration, solvent penetration, water content, solvent content.

1. Introduction

The Epsilon permittivity imaging system which is based on Fujistu fingerprint sensors (Fujistu Ltd), has shown potentials in skin hydration imaging, skin characterization analysis, and skin solvent penetration measurements (Leveque et al., 2003; Batisse et al., 2006; Xiao et al., 2007; Bevilacqua et al., 2008; Singh et al., 2008). It is based on capacitance measurement principles, and the measurement results depend on the sample's dielectric permittivity, because of calibration, we can get the absolute dielectric permittivity so that we can work out the absolute water hydration. Our latest studies showed that Epsilon permittivity imaging system can be used in many solvents, due to their high dielectric permittivity. This makes the technique very useful for in-vivo trans-dermal drug delivery studies (Xiao et al., 2012a; Xiao et al., 2012b).

Preprints (www.preprints.org) | NOT PEER-REVIEWED | Posted: 21 June 2018 doi:10.20944/preprints201806.0331.v1

2. Materials and Methods

2.1 Epsilon permittivity imaging system

The Epsilon permittivity imaging system, based on Fujistu fingerprint sensors (Fujistu Ltd), has 256x300 pixels with 50μm spatial resolution, as shown in **Fig. 1** (Xiao et al., 2012b). Each pixel is equivalent of a capacitive sensor, which measures the dielectric constant or permittivity of the sample. Epsilon has an 8-bit grey-scale capacitance resolution per pixel (0 - 255).

A) Epsilon and the in-vivo stand

B) Epsilon and the in-vitro stand

Preprints (www.preprints.org) | NOT PEER-REVIEWED | Posted: 21 June 2018 doi:10.20944/preprints201806.0331.v1

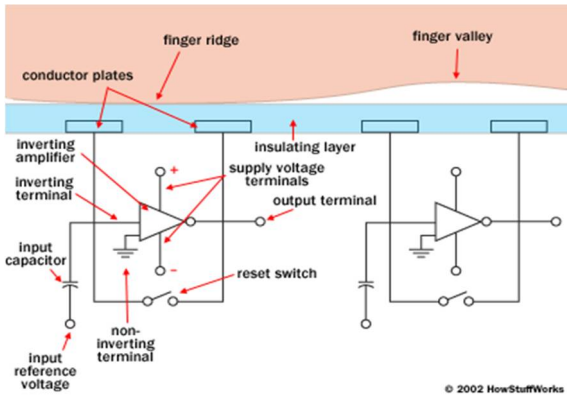

C) Capacitive fingerprint sensor measurement principle [8]

Fig. 1. Epsilon Permittivity Imaging System: A) Epsilon and the *in-vivo* stand, B) Epsilon and the *in-vitro* stand, and C) its measurement principle.

2.2 Epsilon calibration

The Epsilon differs from other similar systems in its calibrated, linear response to near-surface dielectric permittivity, see **Fig. 2**. The linear response is important because hydration is linearly related to permittivity. The calibration ensures consistency from instrument to instrument and from time to time. With calibrated Epsilon imaging systems we can measure the absolute dielectric permittivity of the material. A RGB colour scheme is used to represent the dielectric constant values, the brighter the colour, the higher the dielectric constant, and darker the colour the lower the dielectric constant.

Preprints (www.preprints.org) | NOT PEER-REVIEWED | Posted: 21 June 2018 doi:10.20944/preprints201806.0331.v1

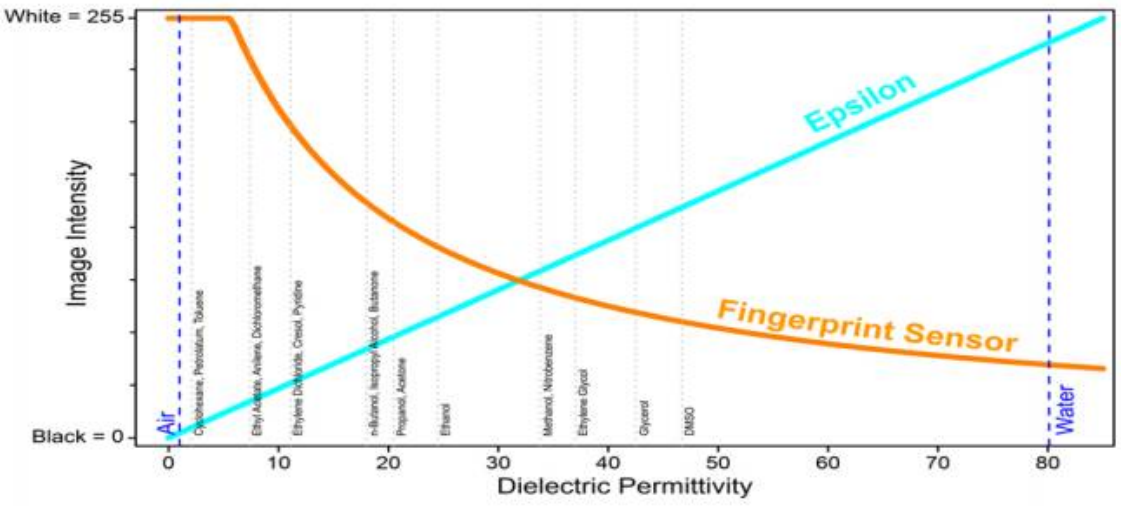

Fig. 2. The Epsilon Calibration curve and linear response to dielectric permittivity

2.3 Skin Hydration and Solvent Concentration Calculations

If we assume measured skin dielectric constant value ($\boldsymbol{\varepsilon}_m$) is linearly dependent on that of dry skin ($\boldsymbol{\varepsilon}_{dry}$) and water ($\boldsymbol{\varepsilon}_{water}$), i.e.

$$\varepsilon_{\mathrm{m}} = \varepsilon_{dry} \times (1 - \frac{H}{100}) + \varepsilon_{water} \times \frac{H}{100} \quad (1)$$

where H is water concentration in skin as percentage of volume ratio, then we can work out the water content using following equation [6]

$$H = \frac{\varepsilon_{\mathrm{m}} - \varepsilon_{dry}}{\varepsilon_{water} - \varepsilon_{dry}} \times 100 \quad (2)$$

For the solvent penetration through skin, measured dielectric constant value ($\boldsymbol{\varepsilon}_m$) is a combination of pure solvent ($\boldsymbol{\varepsilon}_{sol}$) and skin ($\boldsymbol{\varepsilon}_{skin}$), similar to Eq.2, we also can calculate the solvent concentration (**C**, volume ratio percentage),

$$C = \frac{\varepsilon_{\mathrm{m}} - \varepsilon_{skin}}{\varepsilon_{sol} - \varepsilon_{skin}} \times 100 \quad (3)$$

Preprints (www.preprints.org) | NOT PEER-REVIEWED | Posted: 21 June 2018 doi:10.20944/preprints201806.0331.v1

In the paper, the dielectric constants we used for water is $\varepsilon_{water} = 80.1$, for dry skin is $\varepsilon_{dry} = 1$, for pure alcohol is $\varepsilon_{sol} = 24.3$, for pure ethylene glycol is $\varepsilon_{sol} = 55.81$, and for pure glycerol is $\varepsilon_{sol} = 38.91$.

2.4 Re-positioning Using Normalized Cross-Correlation Algorithm

Re-positioning is very important in image processing. In many occasions, we would prefer to compare the results from exactly the same skin site. To select the same skin site manually is cumbersome and inaccurate. We have developed an efficient repositioning technique based on normalized cross-correlation algorithm. As illustrated in **Fig.3.,** users can select the region of interests (RoI) in the first image, the re-positioning technique will automatically find the exactly same position in the subsequent images.

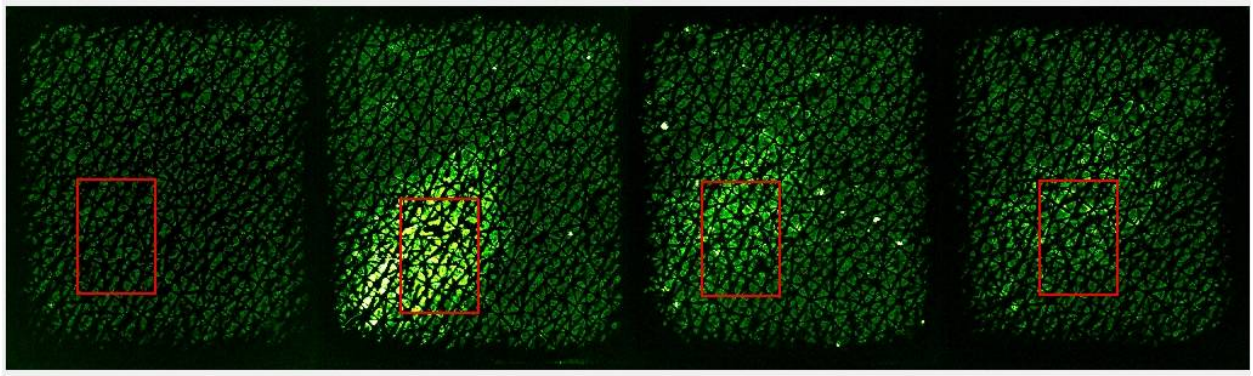

Normal Skin After 0 min 20min 30 min

Preprints (www.preprints.org) | NOT PEER-REVIEWED | Posted: 21 June 2018 doi:10.20944/preprints201806.0331.v1

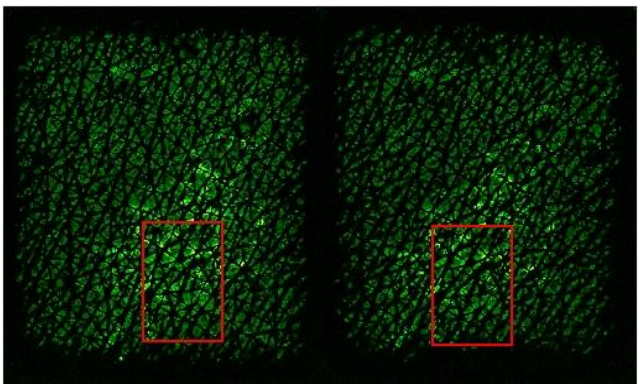

40min 50min

Fig.3. Capacitive contact images of skin before and after Glycerol application. Red squares show the repositioning of the RoI in Normal Skin image (before application) and in the consequent images (after application).

If we use matrix **R** to represent the region of interests, and matrix **T** to represent the target images, we first normalized the **R** using following formula,

$$R_N = \frac{R-min}{max-min} \times 255 \quad (4)$$

Where **max** and **min** are the maximum value and minimum value of **R**, and $\boldsymbol{R_N}$ is the normalized **R**. Similarly we can also normalize **T** to get $\boldsymbol{T_N}$. Then we can calculate the cross-correlation of $\boldsymbol{R_N}$ and $\boldsymbol{T_N}$ as,

$$Corr = \sum_i \left(\frac{\sum_j (R_N(j) - RM) \times (T_N(j-i) - TM)}{\sqrt{\sum_j (R_N(j) - RM)^2} \times \sqrt{\sum_j (T_N(j-1) - TM)^2}} \right) \quad (5)$$

Where **i** and **j** are the matrix indexes, **RM** is the mean of R_N and **TM** is the mean of T_N. From calculation result **Corr** , we can find out at which position that two matrix

Preprints (www.preprints.org) | NOT PEER-REVIEWED | Posted: 21 June 2018 doi:10.20944/preprints201806.0331.v1

are best correlated, and that will be the position of the original region of interests **R** in target image **T**.

2.5 Experimental Procedures

All the measurements were taken under normal ambient laboratory conditions, of 21 ± 1 °C and 45±5 % RH. The volar forearm skin sites from healthy volunteers (aged 20 – 40) were chosen for this study. The volunteers were acclimatized in the laboratory for 20 min prior to the experiments.

For skin characterization, three types of skin damages were studied: intensive washes, tape stripping and sodium lauryl sulphate (SLS) irritation. For intensive washes, room temperature running water and washing-up liquid were used to rub the skin site gently for 3 min with a finger. After wash, the skin site was carefully patted dry with a tissue before the measurements. Tape stripping was performed 20 times per site by the use of standard stripping tape. SLS irritation was achieved by applying 2% SLS water solution (v/v, volume ratio) on skin. Capacitive contact imaging measurements were performed both before and after. The measurements were done by using capacitive imaging sensor to occlude the skin test sites for a period of one minute, during which skin capacitance images were recorded

Preprints (www.preprints.org) | NOT PEER-REVIEWED | Posted: 21 June 2018 doi:10.20944/preprints201806.0331.v1

continuously at the rate of one image per second. The average water contents of the images were then calculated at different times during occlusion using **Eq.2**.

For skin solvent penetration measurements, three solvents were studies, pure ethanol, pure ethylene glycol, and pure glycerol. A small quantity of solvent, held in a plastic well, was applied on skin site for 5 minutes, the skin site was then carefully wiped clean to make sure no solvent residue left on skin surface. The capacitive imaging measurements were performed both before and after the application. Again, the measurements were done by using capacitive imaging sensor to occlude the skin test sites for a period of one minute, during which skin capacitance images were recorded continuously. The solvent concentrations in skin were calculated by using **Eq.4**, and the re-positioning technique was used to make sure the calculations are done on exactly the same skin site.

2. Results and Discussions

2.1 Skin Damage Characterizations

Fig. 4 shows the time dependent skin hydration occlusion curses before and after the intensive wash, tape stripping and SLS irritation. The results show that the levels and the shapes of occlusion curves changed after the skin damage, from the levels

Preprints (www.preprints.org) | NOT PEER-REVIEWED | Posted: 21 June 2018 doi:10.20944/preprints201806.0331.v1

and the shapes we can understand how badly the skin is damaged, and how long does it take to recover. It also is interesting to point out that for different types of skin damages, the time dependent occlusion curves are also different. This suggests that it is possible to use these time dependent occlusion curves to characterize skin, i.e. not only to show how badly the skin is damaged, but also to show what types of damages.

(A)

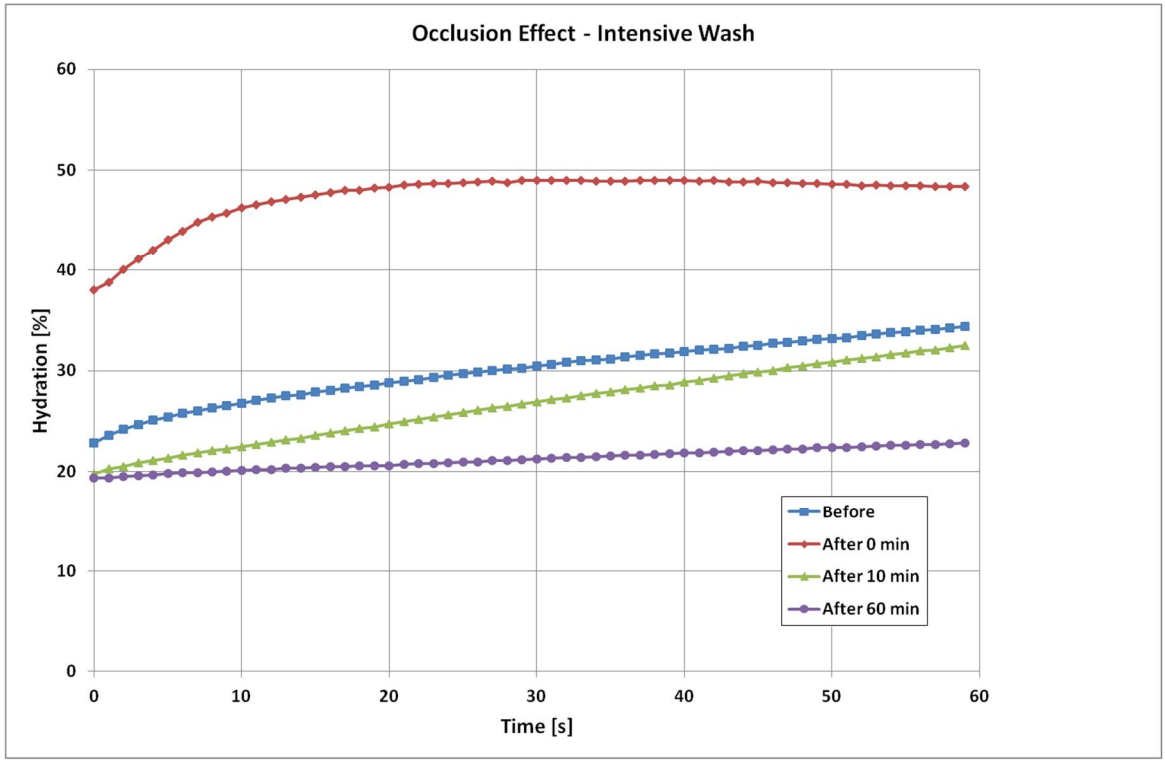

(B)

Preprints (www.preprints.org) | NOT PEER-REVIEWED | Posted: 21 June 2018 doi:10.20944/preprints201806.0331.v1

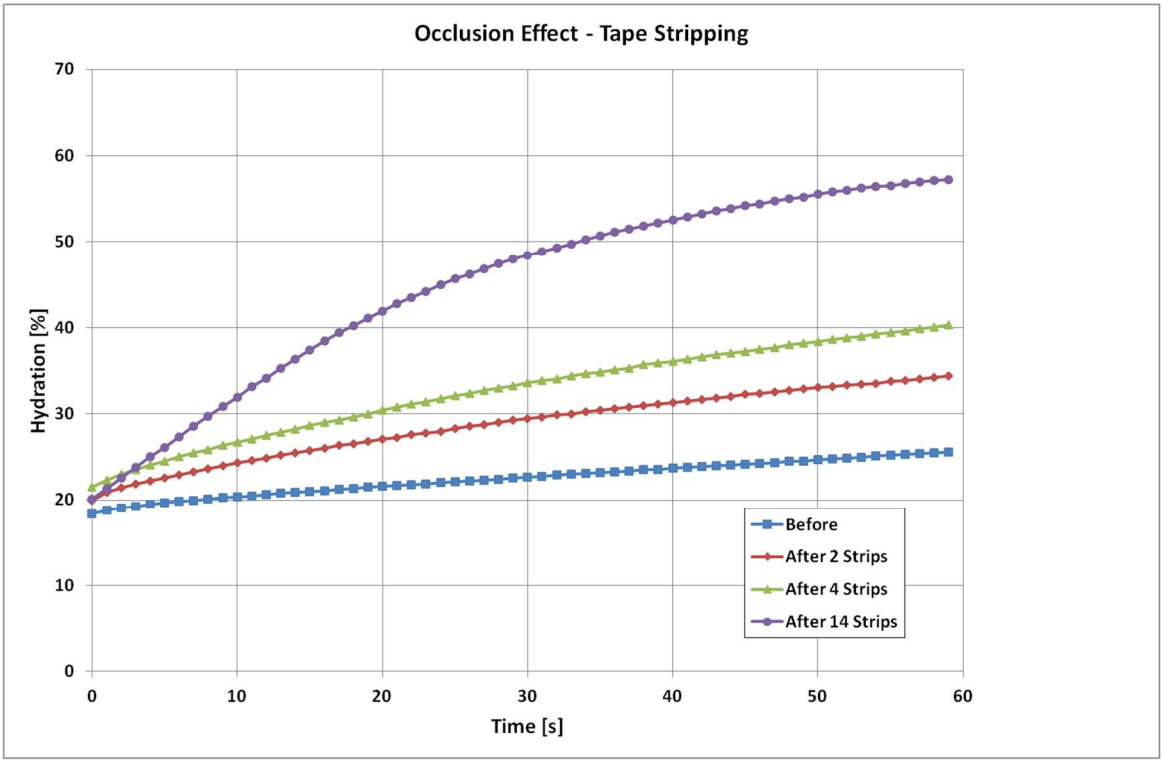

(C)

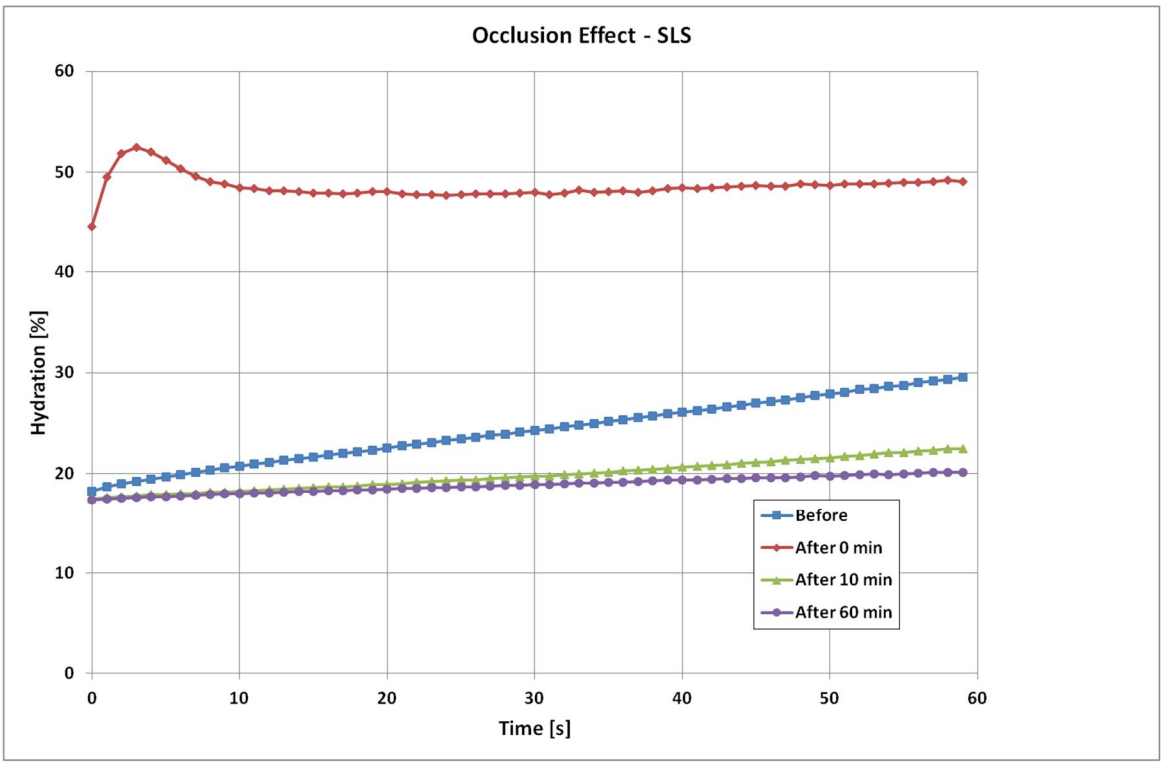

Fig.4. The time dependent skin hydration occlusion curses before and after the intensive wash (A), tape stripping (B) and SLS irritation (C).

Preprints (www.preprints.org) | NOT PEER-REVIEWED | Posted: 21 June 2018 doi:10.20944/preprints201806.0331.v1

Fig. 5 shows corresponding capacitive contact images before and after intensive washes, tape stripping and SLS irritation measurements. The skin images are generally getting brighter after damage, which indicates higher water content in skin. In both intensive washes and SLS irritation, the darker recovery skin images indicate there is a drying effect after the damage.

(A)

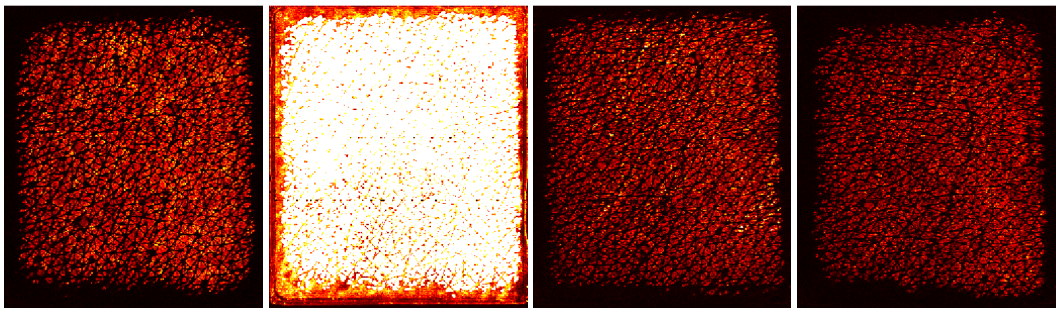

Before After (Wash) 10 min 20 min

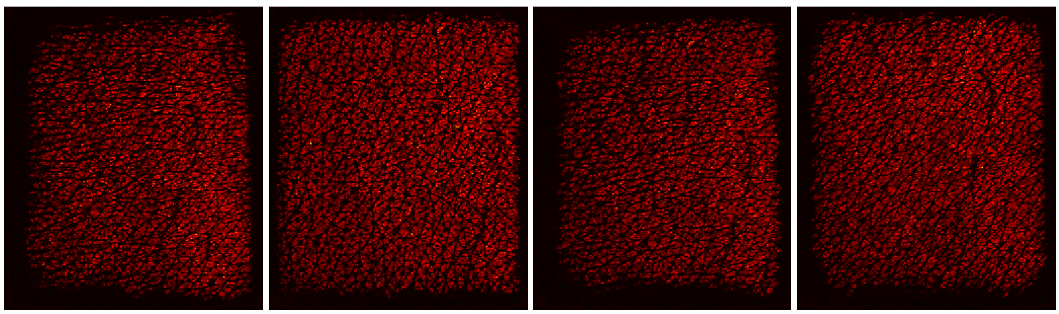

30 min 40 min 50 min 60min

(B)

Preprints (www.preprints.org) | NOT PEER-REVIEWED | Posted: 21 June 2018 doi:10.20944/preprints201806.0331.v1

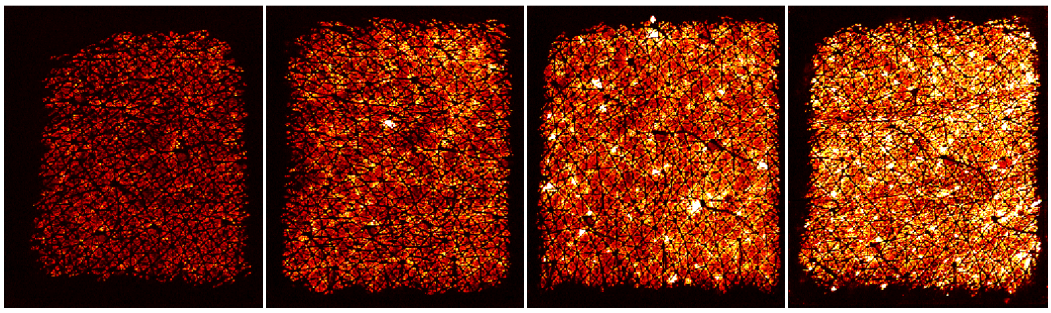

Before After (2strips) 4 strips 6 strips

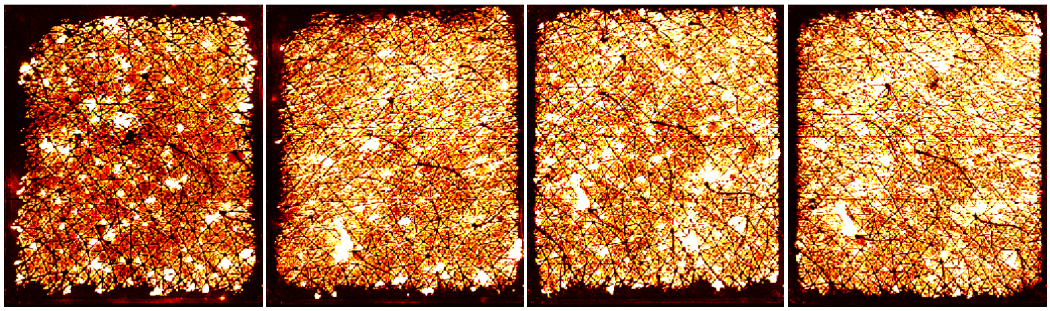

8 strips 10 strips 12 strips 14 strips

(C)

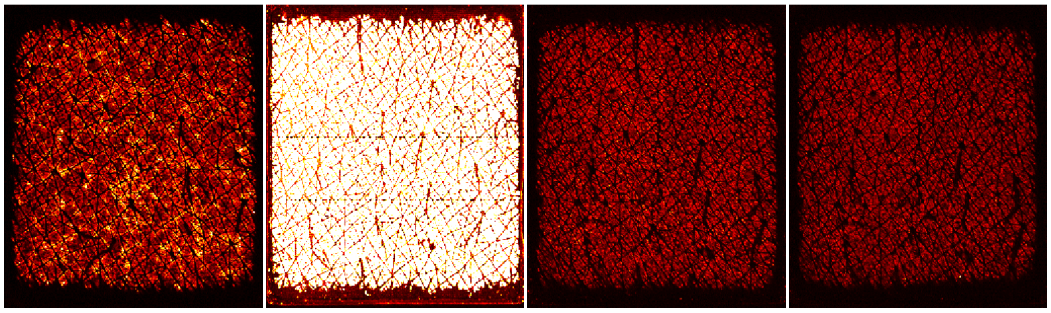

Before After (SLS) 10 min 20 min

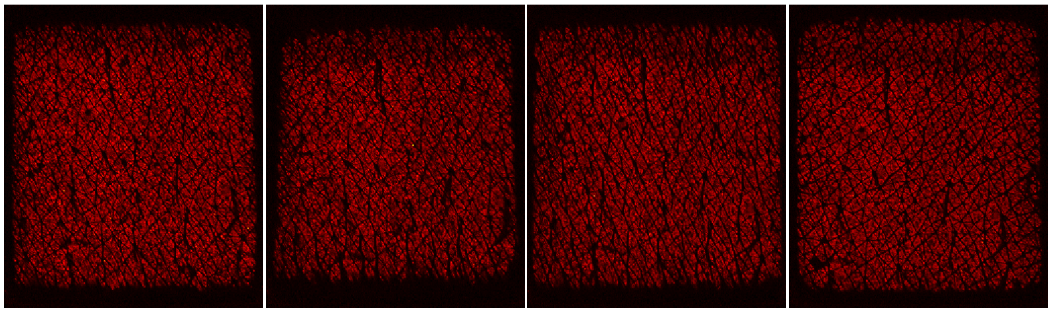

Preprints (www.preprints.org) | NOT PEER-REVIEWED | Posted: 21 June 2018 doi:10.20944/preprints201806.0331.v1

185 30 min 40 min 50 min 60min

186 **Fig. 5.** Typical capacitive contact images of before and after intensive washes (A),

187 tape stripping (B) and SLS irritation (C).

188

189 *2.2 Skin Solvent Penetrations*

190 **Fig. 6** shows the capacitive images before and after the three solvent applications.

191 The image results show that after 5 minutes application, Ethylene Glycol penetrates

192 most into the skin, while Ethanol penetrates the least. This is understandable, as

193 Ethanol is very volatile, and evaporated quickly after the application. Ethylene Glycol

194 also disappears quicker from the skin surface. As Ethylene Glycol is non-volatile, we

195 assume it goes into deeper skin. Glycerol, however, tends to stuck within skin for a

196 long period of time.

197

198 **(A) Ethanol**

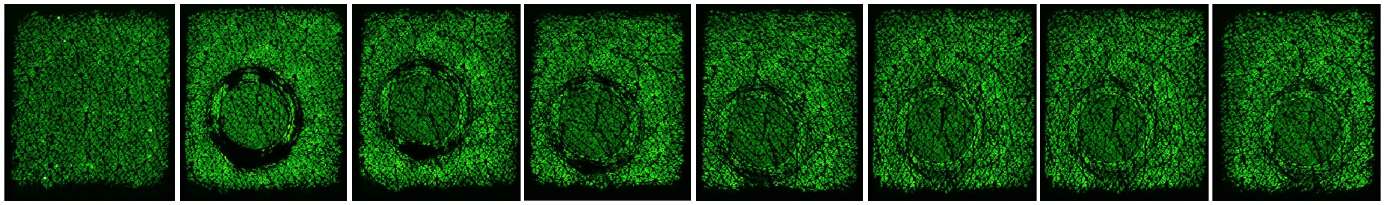

203

Preprints (www.preprints.org) | NOT PEER-REVIEWED | Posted: 21 June 2018 doi:10.20944/preprints201806.0331.v1

204

205 **(B) Ethylene Glycol**

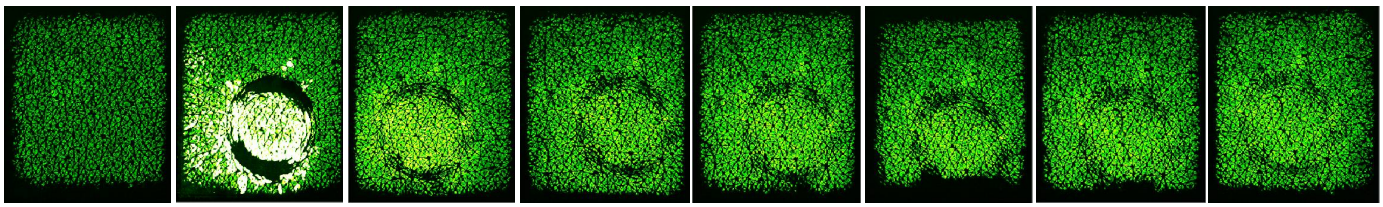

210

211 **(C) Glycerol**

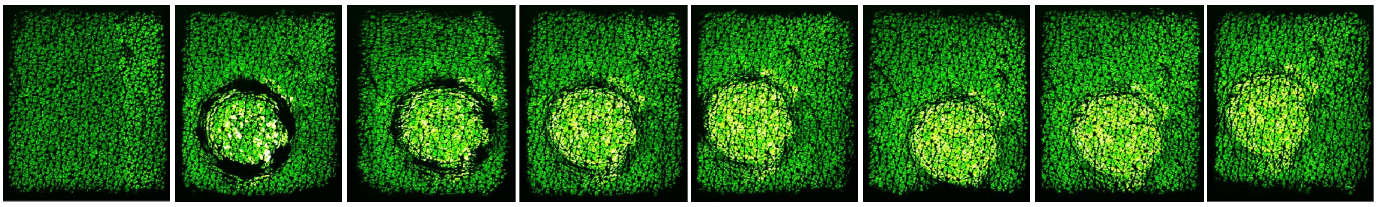

216

217 **Fig. 6.** Capacitive contact images of skin before and after solvent applications, (A)

218 Ethanol, (B) Ethylene Glycol and (C) Glycerol.

219

220 **Fig. 6** shows the corresponding calculated solvent concentration as volume ratio

221 percentage before after solvent applications using Eq.4. The calculated results

Preprints (www.preprints.org) | NOT PEER-REVIEWED | Posted: 21 June 2018 doi:10.20944/preprints201806.0331.v1

222 agree well with the image results. The slight negative undershoots in Ethanol results

223 are likely due to the skin drying because of Ethanol application.

224

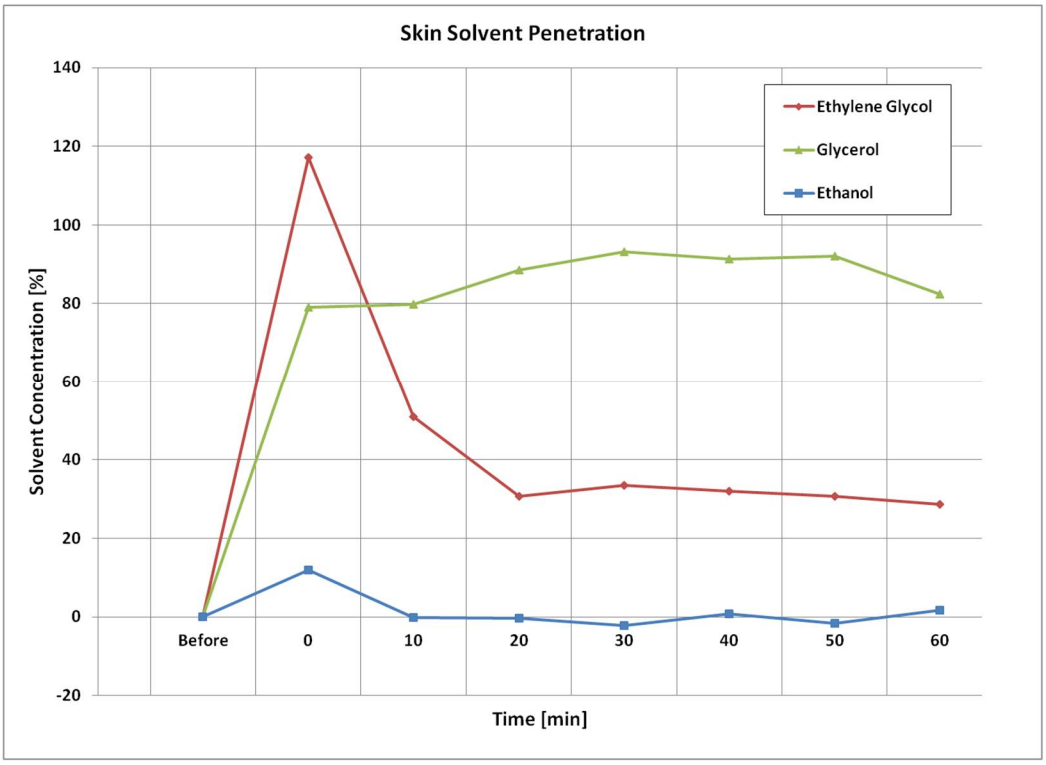

225

226 **Fig. 6.** The calculated solvent concentration as volume ratio percentage before after

227 solvent applications, (A) Ethanol, (B) Ethylene Glycol and (C) Glycerol.

228

229

230

231

232

233

Preprints (www.preprints.org) | NOT PEER-REVIEWED | Posted: 21 June 2018 doi:10.20944/preprints201806.0331.v1

The table below shows the dielectric permittivity of alcohol, ethylene glycol, glycerol, and the concentration of these 3 solvents in the skin from base site to 60 minutes (base site to t6, every 10 minutes).

Figure 6 shows a 5min Glycerol application measurement. Similarly, we can use $C=(\varepsilon - \varepsilon skin)/(\varepsilon Glycerol - \varepsilon skin)$ to work out the Glycerol concentration. By using re-positioning technique (RoI + cross correlation), we can select exactly the same skin region we want to analyse in each image, see following red squares. The results show that Glycerol in skin has reached to ~38% (v/v) after just 5min Glycerol application. Then as Glycerol gradually diffuse into to skin, the concentration reduced to 16% (20 min), 9% (30min), 10% (40min) and 6% (50 min).

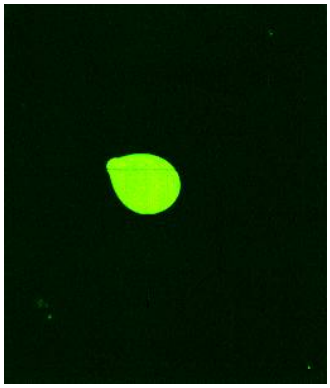

Glycerol

4 Conclusions

 doi:10.20944/preprints201806.0331.v1

The result shows that, because of volatilizing, the permittivity of alcohol decreased, after t0 (t1-t6), and the capacitive images become darker than base site, the permittivity of both ethylene glycol and glycerol much more increased than base site and diffusion under the surface, the capacitive images of these 2 solvents become brighter than base site, but we can notice the different between these 2 solvents, ethylene glycol is absorbed faster than glycerol.

Acknowledgement

We thank London South Bank University for the financial support.

References

1. Léveque, J.L. and Querleux, B. SkinChip, a new tool for investigating the skin surface in vivo. Skin Research and Technology 9, 343-347, (2003).

2. Batisse, D., Giron F. and Léveque J.L. Capacitance imaging of the skin surface. Skin Research and Technology 12, pp99-104, (2006).

3. Xiao P, Singh H, Zheng X, Berg EP, Imhof RE, In-vivo Skin Imaging For Hydration and Micro Relief Measurements. SCV Conference, Cardiff, UK, July 11-13, 2007.

4. Ou, X., Pan, W., Xiao, P., In vivo skin capacitive imaging analysis by using grey level co-occurrence matrix (GLCM), International Journal of Pharmaceutics, November 2013, ISSN 0378-5173, http://dx.doi.org/10.1016/j.ijpharm.2013.10.024.

5. W. Pan, X. Zhang, M.E. Lane and P. Xiao, "The Occlusion Effects in Capacitive Contact Imaging for In-vivo Skin Damage Assessments", International Journal of Cosmetic Science, 2015, 37, 395–400, doi: 10.1111/ics.12209.

6. P. Xiao, C. Bontozoglou, Capacitive contact imaging for in-vivo hair and nail water content measurements, H&PC Today, Vol. 10(5), pp62-65, September/October 2015.

7. W. Pan, X. Zhang, E. Chirikhina and P. Xiao, "Skin Hydration Measurement Using Contact Imaging", SCC Showcase, New York, December 11 - 12, 2014.

8. Fujitsu Fingerprint Sensor, http://edevice.fujitsu.com/fj/MARCOM/find/20-1e/pdf/001.pdf

Baraldi, A.. (1995, Mar.). An investigation of the textural characteristics associated with gray level cooccurrence matrix statistical parameters. Geoscience and Remote Sensing, IEEE Transactions on. 33(2), pp. 293 – 304.

Batisse, D., Giron F. and Leveque J.L. Capacitance imaging of the skin surface. Skin Research and Technology 12, pp99-104, (2006).

Bevilacqua, A. Gherardi, A., Characterization of a capacitive imaging system for skin surface analysis, First International Workshops on Image Processing Theory, Tools & Applications, 23-26 Nov, 2008.

292 Conners, Richard W. (1980, May). A Theoretical Comparison of Texture Algorithms.
293 Pattern Analysis and Machine Intelligence, IEEE Transactions on. PAMI-2(3), pp.
294 204 – 222.
295 Gao, ChengCheng and Hui, Xiaowei, (2010, Oct.) GLCM-based Texture Feature
296 Extraction, Computer Systems & Applications, 2010, 19(6), pp 195-198.
297 Haralick, R.M. (1973, Nov.). Textural Features for Image Classification. Systems,
298 Man and Cybernetics, IEEE Transactions on. SMC-3(6), pp. 610 – 621.
299 Haralick, R.M. (1973, Oct.). Computer Classification of Reservoir Sandstones.
300 Geoscience Electronics, IEEE Transactions on. 11(4), pp. 171 – 177.
301 Haralick, R.M. (1979, May). Statistical and structural approaches to texture.
302 Proceedings of the IEEE. 67(5), pp. 786 – 804.
303 Kekre, H.B., Thepade, S.D., Sarode, T.K. and Suryawanshi, V., (2010, October).
304 Image Retrieval using Texture Features extracted from GLCM, LBG and KPE.
305 International Journal of Computer Theory and Engineering. 2(5), pp. 1793-8201.
306 Leveque, J.L. and Querleux, B. SkinChip, a new tool for investigating the skin
307 surface in vivo. Skin Research and Technology 9, 343-347, (2003).
308 Parekh, Ranjan. (2012, Feb.). Using Texture Analysis for Medical Diagnosis.
309 MultiMedia, IEEE. 19(2), pp. 28 – 37.

310 Rafael C. Gonzalez and Richard E. Woods. (2007, August 31). Digital Image
311 Processing Third Edition. Prepared by Pearson Education. pp. 142-161.
312 Siew, Lee Hok . (1988, Jan). Texture measures for carpet wear assessment. Pattern
313 Analysis and Machine Intelligence, IEEE Transactions on. 10(1), pp. 92 – 105.
314 Singh, H., Xiao, P., Berg, E.P., and Imhof, R.E., Skin Capacitance Imaging for
315 Surface Profiles and Dynamic Water Concentration Measurements, ISBS
316 Conference, Seoul, Korea, May 7-10, 2008.
317 Tahir, M. A..(2003, 14-17 Dec.). An FPGA based co-processor for GLCM texture
318 features measurement. Electronics, Circuits and Systems, 2003. ICECS 2003.
319 Proceedings of the 2003 10th IEEE International Conference on. 3, pp. 1006 –
320 1009.
321 Ulaby, F.T., Kouyate, F., Brisco, B., Williams, T.H.L., IEEE Transactions On
322 Geoscience And Remote Sensing, Vol. GE-24, NO. 2, March 1986, pp 235 – 245.
323 Xiao, P., Singh, H., Zheng, X., Berg E.P., and Imhof, R.E., In-vivo Skin Imaging For
324 Hydration and Micro Relief Measurements, Stratum Corneum V conference, July
325 11-13, 2007, Cardiff, UK.
326 Xiao, P., Lane, M.E., and Abdalghafor, H.M., Membrane Solvent Penetration
327 Measurements using Contact Imaging, Stratum Corneum VII Conference, Cardiff,
328 UK, Sep 10-12, 2012.

329 Xiao, P., Ou, P., Ciortea, L.I., Berg E.P., and Imhof, R.E., “In-vivo Skin Solvent
330 Penetration Measurements Using Opto-thermal Radiometry and Fingerprint
331 Sensor”, International Journal of Thermophysics, 33:1787–1794, DOI
332 10.1007/s10765-012-1318-6, 2012.
333 Zhu, Le-qing. (2010, 10-12 Aug.). Auto-classification of insect images based on color
334 histogram and GLCM. Fuzzy Systems and Knowledge Discovery (FSKD), 2010
335 Seventh International Conference on. 6, pp. 589 – 2593.